

# Noninvasive monitoring of cerebral blood flow by a dye bolus method: Separation of brain from skin and skull signals

**Matthias Kohl-Bareis**

Humboldt University  
Charité Hospital  
Department of Neurology  
Schumannstrasse 20/21  
10117 Berlin, Germany  
and  
University of Applied Sciences Koblenz  
Rhein Ahr Campus  
Suedallee 2  
53424 Remagen, Germany

**Hellmuth Obrig**

**Jens Steinbrink**

**Jasmin Malak**

**Kamil Uludag**

**Arno Villringer**

Humboldt University  
Charité Hospital  
Department of Neurology  
Schumannstrasse 20/21  
10117 Berlin, Germany

**Abstract.** Tracking a bolus of contrast agent traveling through the cerebral vasculature provides a measure of the blood flow velocity in the respective cerebral tissue. This principle has been the basis for the first approaches in functional magnetic resonance (MR) imaging and is of great value for investigating patients with vascular disease, especially stroke. While bolus measurements are a standard procedure in MR imaging, optical bolus tracking is as yet not established. Here we study optical absorption changes induced by a bolus of the dye indocyanine-green with near infrared spectroscopy in healthy volunteers. The aim is to assess the latency and shape of the change in absorption. Since application in the adult human critically depends on differentiation between extra- and intracerebral vascular compartments we focus on an approach for such a separation. To do this frequency-domain and multidistance measurements are analyzed by a Monte Carlo based model for photon transport in tissue. Based on measurements of both the photon's mean time of flight (phase) and the intensity, our results allow differentiation between an upper (skin and skull) and a lower layer (brain). The bolus in the deeper tissue layers has a peak of about 10 s width, while the change in absorption in the upper layers shows a much longer recovery time. This is in qualitative agreement with MR imaging results using a gadolinium bolus. This result is promising with respect to the potential of bedside monitoring of mean transit time (MTT) changes in patients with stroke or related vascular disease. © 2002 Society of Photo-Optical Instrumentation Engineers. [DOI: 10.1117/1.1482719]

**Keywords:** NIRS; ICG; cerebral perfusion; frequency-domain spectroscopy; Monte Carlo Simulation.

Paper JBO 01065 received Sep. 20, 2001; revised manuscript received Feb. 7, 2002; accepted for publication Feb. 11, 2002.

## 1 Introduction

Cerebral perfusion is a key parameter for the monitoring of cerebral ischemia. Position emission tomography (PET), magnetic resonance imaging (MRI), and lately also computer tomography (CT) can approximate this parameter with different tracer and bolus techniques. However, they rely on complex equipment and cannot be used at the bedside. Potentially, near infrared spectroscopy (NIRS) offers an inexpensive bedside monitoring tool when used for tracking an optical dye bolus. The reasoning is that the arrival time, i.e., the delay between the bolus signal and the time of intravenous injection and the shape (width) of the bolus allow perfusion parameters to be reliably approximated.

For the last few years the optical dye indocyanine green (ICG) has been used in NIRS bolus measurements. When ICG signals are measured in babies and children, the bolus peak is less than 10 s in width.<sup>1–3</sup> In this case Fick's principle is applied to quantify the blood flow. Based on an experimental study in pigs, Kuebler et al.<sup>4</sup> derived a so-called blood flow

index from the initial slope of the bolus signal. Alternatively, measurements of the ICG bolus signals at the inlet (aorta) and the outlet (jugular bulb) of the brain were exploited for perfusion quantification.<sup>5,6</sup> However, this provides a measure of the global cerebral blood flow only.

The key obstacle to wide application of NIRS bolus methods in adults is the limited photon penetration depth into the tissue. On the one hand, this will always restrict the detection of perfusion impairments to the upper cortical layers when applied to adults. Also, the optical data will contain a signal not only from the cortex but one from the skin and skull as well. Therefore a method by which to separate the intracranial signal from extracranial contamination is required. This problem is obviously less severe in flow monitoring of babies or young children where the skull is considerably thinner.

The problem of extracerebral signals is highlighted by analyzing standard MR-bolus signals using gadolinium-DTPA as the contrast agent. In Figure 1 extra- and intracerebral bolus signals measured in a healthy volunteer are compared. The intracerebral time course [Figure 1(b)] at the six measurement

Address all correspondence to Matthias Kohl-Bareis. Tel: +49 2642 932 342; Fax: +49 2642 932 399; E-mail: kohl-bareis@rheinahr-campus.de

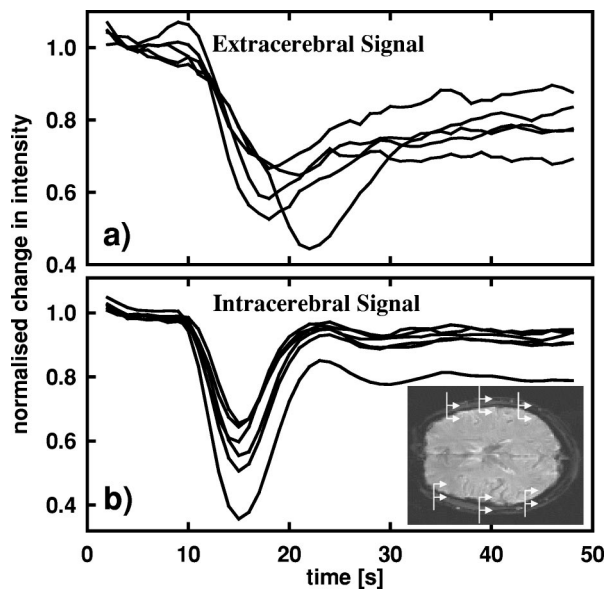


**Fig. 1** Time courses of MRI perfusion signals using Gd-DTPA as a tracer normalized at the time of injection ( $t=0$  s). Bolus signals were (a) analyzed at six extracerebral sites and (b) compared to those of adjacent intracerebral sites (marked by the arrows in the inset).

positions (cf. the inset of Figure 1) has a minimum at  $t = 15$  s with a width [full width at half maximum (FWHM)]  $< 10$  s. In contrast, the extracerebral signal [Figure 1(a)] has a different shape with a peak delayed by a few seconds and a much slower recovery to the baseline. These extracerebral signals strongly depend on the measurement position. We found similar shapes in all volunteers analyzed. It is obvious that these different time courses impose a problem for perfusion measurements performed by NIRS.

To solve this problem and to establish NIRS perfusion measurements, it has been suggested that one should subtract the signal/attenuation changes received from different source–detector positions. This is based on the assumption that light traveling through the extracranial tissue is almost identical for all source–detector distances.<sup>7</sup> Moreover, McCormick et al. injected ICG boli into both the exposed internal carotid artery (ICA) and the external carotid artery (ECA).<sup>8</sup> When detecting at detector spacings of 1 and 2.7 cm, a bolus injected into the ECA resulted in a similar time course and magnitude in both detectors, while injection into the ICA was followed by a signal at larger detector spacing only.

The major approach we follow in this paper is based on the observation that different measurement parameters like intensity and photon time of flight have different sensitivity to different depths of tissue.<sup>9,10</sup> Therefore such measurements do provide information on the separation of extra- and intracerebral signal. The main objective of this paper is to find out whether frequency-domain or multidistance measurements can help to better separate extra- from intracerebral absorption changes. The concept is that the photon mean time-of-flight parameter (phase) obtained from the frequency-domain technique is more sensitive to absorption changes in deeper tissue layers than intensity measurements. This sensitivity is estimated from a physical model for light transport in tissue based on Monte Carlo simulations. In principle time-domain

measurements contain the maximum amount of available information for a depth resolved measurement.<sup>11,12</sup> Here we limit ourselves to frequency domain and the following questions. (1) Is the information contained in the two measurement parameters, intensity and mean time of flight (phase) sufficient for signal separation? (2) How reliable is this separation when the basic assumption for the underlying model of photon transport is varied? (3) For its lower demand on instrumentation, multidistance intensity-only measurements seem preferable. Its potential use for the separation of cortical ICG bolus measurements is therefore examined as well.

## 2 Methods

### 2.1 Experimental Setup

A frequency-domain spectrometer (ISS Inc., Champaign, Illinois) working at a modulation frequency of 110 MHz was used to measure changes in attenuation and phase, an equivalent to mean photon transit time ( $\langle t \rangle$ ). The wavelengths chosen (780 or 810 nm) are close to the absorption maximum of ICG. Data were acquired at a source–detector separation of  $r = 3$  cm at a sampling rate of  $f = 3$  Hz.

Reflectance spectra were recorded with a spectrometer coupled charge coupled device (CCD) camera (Princeton Instruments; Acton Research) at a frequency of 4 Hz. Detector fibers were positioned in a line 10, 20, 30, and 40 mm from the delivering fiber that was connected to a halogen light source (filtered to 700–1000 nm). Attenuation changes were converted into concentration changes in oxygenated and deoxygenated hemoglobin as well as ICG based on a modified Lambert–Beer approach that takes into account the wavelength dependence of the total optical pathlength [differential pathlength factor (DPF)] provided by Matcher et al.<sup>13</sup> The ICG absorption spectrum given by Roberts et al. was used.<sup>2</sup> Because the absolute pathlength (in mm) is not known, concentration changes are given in units of  $\mu\text{M mm}$ .

Twelve NIRS bolus experiments were performed in adult volunteers with typically five ICG bolus injections separated by 2–3 min each. Boli of 5 mg indocyanine green (ICG), (Pulsion GmbH, Germany) in 3 mL water were manually applied to the cubital vein (injection time  $\sim 1$  s). Measurements were made at different locations over the occipital, parietal, or frontal regions of the subject's head.

Gadolinium-DTPA bolus measurements were performed in four healthy, adult volunteers with a 1.5 T MRI scanner (Siemens Vision, Erlangen, Germany).  $T_2$  relaxation times were recorded following an intravenous injection of the Gd tracer (Magnevist, Schering, Germany). Intracerebral signal time courses were analyzed over regions close to the skull. The extracerebral signals were calculated over areas of the skin and skull; in this case the signal to noise (S/N) ratio is low due to the suppression of fat in the  $T_2$  sequence used.

### 2.2 Depth Resolved Analysis

NIRS intensities ( $I$ ) were converted into attenuation changes  $\Delta A = \log(I_0/I)$ , where  $I_0$  is the intensity at  $t=0$  s (injection time). Changes in phase  $\Delta\Phi$  (in degrees) are equivalent to changes in the mean time of flight  $\Delta\langle t \rangle$ ,<sup>14</sup>

$$\Delta\langle t \rangle = \Delta\Phi / (\nu_M \cdot 360^\circ), \quad (1)$$

where  $\nu_M$  is the modulation frequency (110 MHz) of the spectrometer. The conversion of the recorded changes of  $\Delta A$  and  $\Delta\langle t \rangle$  into changes in absorption coefficient  $\Delta\mu_a$  (i.e., the ICG concentration) is based on the following assumption. First, the tissue is separated into an upper and a lower compartment separated at depth  $z_s$  with (unknown) absorption changes  $\Delta\mu_{a,low}$  and  $\Delta\mu_{a,up}$ . Second, the experimental measurement parameters  $\Delta A$  and  $\Delta\langle t \rangle$  are written as

$$\Delta A = l_{low} \cdot \Delta\mu_{a,low} + l_{up} \cdot \Delta\mu_{a,up}, \tag{2}$$

$$\Delta\langle t \rangle = m_{low} \cdot \Delta\mu_{a,low} + m_{up} \cdot \Delta\mu_{a,up}.$$

Here,  $l_{low}$ ,  $l_{up}$ ,  $m_{low}$ , and  $m_{up}$  are the sensitivities of  $A$  and  $\langle t \rangle$  with respect to changes in  $\mu_a$  in the lower and upper compartments. Based on these equations,  $\Delta\mu_a$  can readily be obtained for both compartments once  $l_j$  and  $m_j$  are known and  $\Delta A$  and  $\Delta\langle t \rangle$  are measured.

Monte Carlo (MC) simulations were performed to estimate the sensitivity factors  $l_j$  and  $m_j$  for layered media. Details of the procedure are found in papers by Steinbrink et al. and by Uludag et al.<sup>11,12,15</sup>  $l_j$  is equivalent to the (mean) optical pathlength of the photons in tissue layer  $j$  ( $j$  for low or up) and is calculated from

$$l_j = \sum_i l_{ij} W_i / \sum_i W_i, \tag{3}$$

where  $W_i$  is the survival weight of the  $i$ th photon bundle that reaches the detector and  $l_{ij}$  is the pathlength of the  $i$ th photon bundle in layer  $j$ . The summation is over all photon bundles ( $i$ ). In a homogeneous medium,  $m_j$  corresponds to the variance in photon temporal distribution  $m_j = (\langle t \rangle^2 - \langle t^2 \rangle) \cdot v_j$ , where  $v_j$  is the velocity of light in layer  $j$ . In an inhomogeneous medium it is<sup>11</sup>

$$m_j = l_j \cdot \langle t \rangle - \sum_k \frac{l}{v_k} \langle l_k l_j \rangle, \tag{4}$$

where the cross term is

$$\langle l_k l_j \rangle = \frac{\sum_i l_{ij} l_{ik} W_i}{\sum_i W_i}.$$

The medium was assumed to consist of nine layers 2 mm thick followed by a semi-infinite half space. The medium was homogeneous, i.e., it had the same tissue optical properties ( $\mu_a, \mu'_s, n$ ) independent of the depth. Anatomical structures such as the skull or the cerebro-spinal fluid (CSF) were disregarded. Photons (typically  $4.2 \times 10^7$ ) were launched at one position and the photons reflected were detected in concentric rings 3 mm in width at various distances from the source. Scattering anisotropies were disregarded. The refractive index of the medium was  $n = 1.4$ . Fresnel reflection at the boundary of the medium was not included. The survival weight of the detected photons was calculated as well as the pathlength distribution (equivalent to the time distribution) for each layer.

In Figure 2  $l_j$  and  $m_j$  are plotted for the layered medium assuming  $\mu'_s = 1 \text{ mm}^{-1}$  and  $\mu_a = 0.01, 0.02, \text{ and } 0.03 \text{ mm}^{-1}$ . These  $\mu_a$  values sufficiently cover the range expected for biological tissue in the NIR wavelength range.  $l_j$  is given for

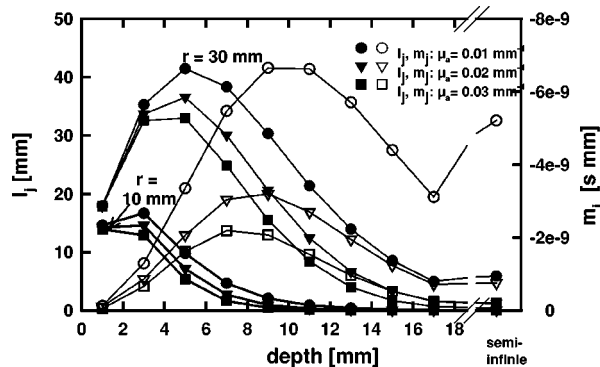


**Fig. 2** Sensitivity of attenuation ( $l_j$ ; closed symbols) and mean time of flight ( $m_j$ ; open symbols) with respect to changes in  $\mu_a$  in a layer of thickness 2 mm at various depths based on Monte Carlo simulations.  $\mu'_s = 1 \text{ mm}^{-1}$  and  $\mu_a$  values of 0.01, 0.02, and 0.03  $\text{mm}^{-1}$  were assumed. Source–detector distances of  $r = 10$  and 30 mm were chosen for  $l_j$  and  $r = 30$  mm for  $m_j$ .

source–detector distances of  $r = 10$  and 30 mm, while  $m_j$  is plotted for  $r = 30$  mm only. It is apparent that measurements of  $\langle t \rangle$  are more sensitive to variations of  $\Delta\mu_a$  in deeper layers. While  $l_j$  has the highest sensitivity in the layer with depth between 4 and 6 mm with regard to  $r = 30$  mm,  $m_j$  peaks for the layer at 8–10 mm depth. By choosing a short source–detector distance of 10 mm, the sensitivity of  $l_j$  to changes at depth  $> 8$  mm is very low. For the analysis outlined in Eq. (2), the sensitivities of the lower and upper compartments separated at a depth  $z_s$  were obtained by adding the  $l_j$  and  $m_j$  values for  $z < z_s$  and  $z > z_s$ , respectively. Similar to in Eq. (2), a separation of the upper and lower absorption changes based on attenuation measurements ( $\Delta A_{r1}, \Delta A_{r2}$ ) at different source–detector separations,  $r_1$  and  $r_2$ , is theoretically feasible when the pathlength in the layers ( $l_{low,r1}, l_{low,r2}, l_{up,r1}$ , and  $l_{up,r2}$ ) are included. The whole set of estimated values of  $l_j$  and  $m_j$  as a function of the depth for  $0.01 \text{ mm}^{-1} < \mu_a < 0.07 \text{ mm}^{-1}$ ,  $1 \text{ mm}^{-1} < \mu'_s < 3 \text{ mm}^{-1}$ , and  $6 \text{ mm} < r < 60 \text{ mm}$  can be obtained from the authors.

Equations (2)–(4) are based on the linear approximation which is accurate only when the fractional change in  $\mu_a$  is small. Estimation of higher order terms with sufficient signal to noise ratio would require considerably more computational time in the MC simulation so it was not considered here. Therefore we have no means by which to estimate the error when the fractional change in  $\mu_a$  is of the order of 20%–30% as calculated for the experiments discussed below.

### 3 Results

Models for the separation of ICG concentrations into different tissue compartments based on a single wavelength analysis require that there are no concurrent changes in hemoglobin. This was tested by spectral analysis of attenuation changes within the range of 740–880 nm. An example is given in Figure 3(a) where the changes in hemoglobin concentration (deoxy-Hb, oxy-Hb) and ICG are plotted for the time period following three bolus injections. There are fluctuations in the hemoglobin traces, however, within the noise level they are not correlated with the ICG bolus. This is apparent from the bolus attenuation spectrum [see Figure 3(b)] that closely fits

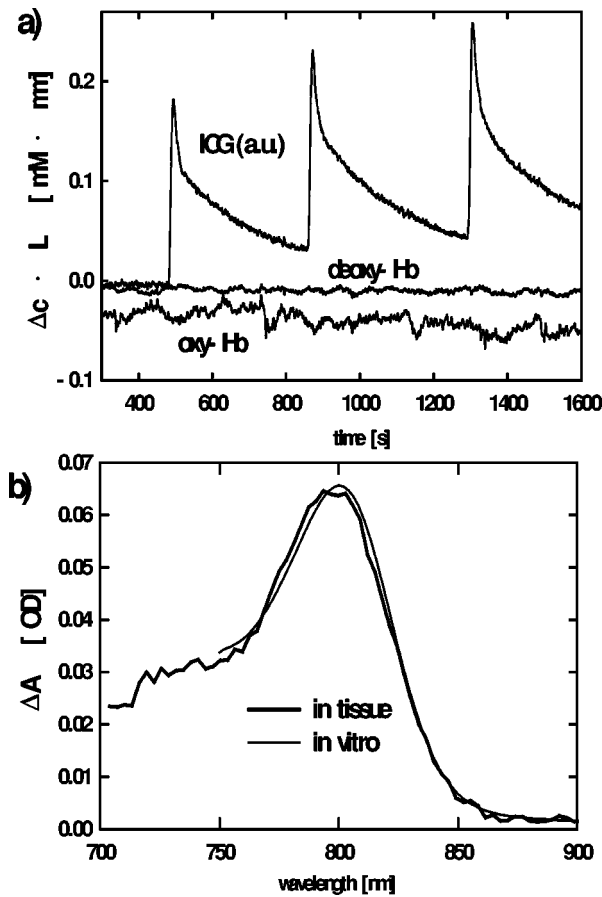


**Fig. 3** (a) Calculated concentration changes in ICG, oxy-Hb, and deoxy-Hb following three ICG bolus injections. For ICG the values are arbitrarily scaled. (b) Attenuation spectrum averaged over the period of the first ICG signal ( $t=490\text{--}570$  s). For comparison, the arbitrarily scaled *in vitro* absorption spectrum of ICG is shown.

the *in vitro* ICG absorption spectrum. The small discrepancies in the peak absorption wavelength are due to uncertainties in the ICG absorption spectrum itself or to the wavelength dependence of the optical pathlength. The *in vitro* ICG absorption spectrum is not corrected for the wavelength dependence of the optical pathlength since the major ICG signal contribution originates from the upper tissue layers. In these compartments the effect of the wavelength dependent absorption spectrum on the pathlength is small and was therefore neglected.

An example of the bolus time course measured with the frequency-domain spectrometer in a volunteer is given in Figure 4. Averaged data of six consecutive ICG injections are shown for a source–detector separation of 30 mm at  $\lambda = 780$  nm. The maximum change in attenuation [Figure 4(a)] is reached about 27 s after injection. As already seen in Figure 3 for the ICG trace, the recovery to baseline values is slow with an initially faster decay. The  $\langle t \rangle$  time course rises a few seconds earlier and peaks about 22 s after injection. Note that the mean time of flight signal decreases (at the peak,  $\Delta\langle t \rangle = -23$  ps), consistent with a rise in the absorption coefficient. For  $t > 40$  s, the recovery to the baseline of  $\Delta A$  and  $\Delta\langle t \rangle$  is very similar. The bolus signals ( $\Delta\mu_a$ ) for an upper compartment (0–12 mm) and a lower compartment ( $>12$  mm) were calculated from these data based on Eq. (2) and are shown in

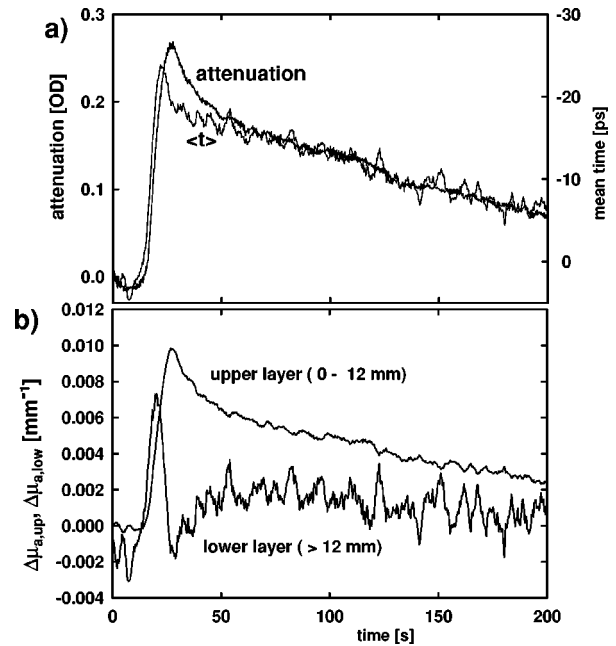


**Fig. 4** (a) Measured change in attenuation and mean time of flight averaged over six consecutive injections of ICG. (b) Conversion of the data in (a) into changes in absorption coefficient of an upper and a lower compartment based on the assumption  $\mu_a = 0.02 \text{ mm}^{-1}$ ,  $\mu'_s = 1 \text{ mm}^{-1}$  and that the upper compartment has a thickness of 12 mm and the lower compartment is semi-infinite.

Figure 4(b). A transport scattering coefficient of  $\mu'_s = 1 \text{ mm}^{-1}$  and an absorption coefficient of  $\mu_a = 0.02 \text{ mm}^{-1}$  were assumed for estimation of  $l_j$  and  $m_j$ . To separate the lines in Figure 4(b), the baseline of  $\Delta\mu_{a,low}$  was shifted by  $-0.002 \text{ mm}^{-1}$ . The signal of the lower compartment peaks at about 20 s with a FWHM of  $\approx 10$  s, followed by a slower recovery to the baseline ( $t \approx 30$  s). In contrast, the  $\Delta\mu_a$  time course of the upper compartment is delayed with a slower recovery to the baseline. These differences closely resemble those of the Gd bolus for the extra- and intracerebral compartments shown in Figure 1.

The obvious question is whether the calculated time course of  $\mu_a$  is affected by basic assumptions of the tissue optical properties and the layer geometry. In Figure 5 the calculated  $\mu_a$  changes are shown for the two compartments when the thickness of the upper compartment ( $z_s$ ) is varied between 6 and 18 mm. The calculations are based on the experimental data shown in Figure 4(a). In all cases  $\mu'_s = 1 \text{ mm}^{-1}$  and  $\mu_a = 0.02 \text{ mm}^{-1}$  were assumed. The results indicate that variation of  $z_s$  has only a minor effect on the shape of the  $\Delta\mu_a$  time course of the upper compartment whereas the magnitude increases with an increase of  $z_s$ . The  $\Delta\mu_a$  time course of the lower compartment has a clear bolus peak in all cases. However, for  $z_s \leq 8$  mm the recovery to the baseline is incomplete for times  $> 25$  s. For  $z_s \geq 14$  mm the calculated  $\Delta\mu_a$  changes (i.e., ICG concentration changes) are negative for  $t > 25$  s. This is clearly unreasonable for an increase in dye concentration, and puts a theoretical limit on depth penetration.

Next, the influence of the assumed background tissue absorption coefficient was examined. Figure 6 gives the results

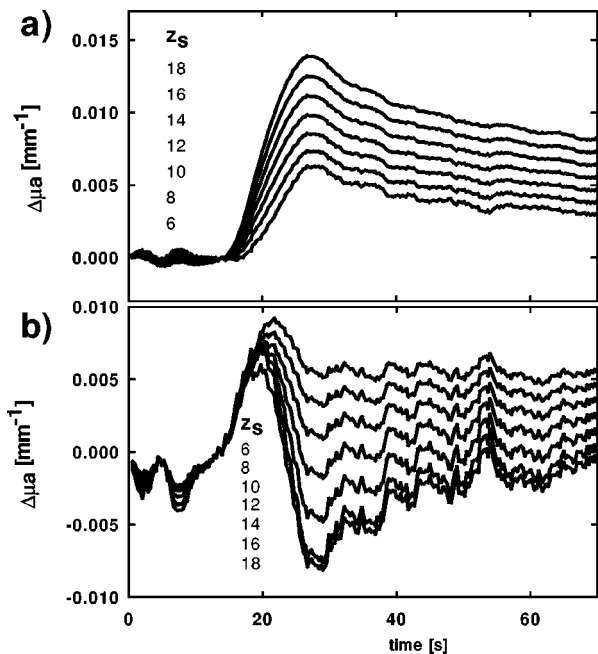


**Fig. 5** Calculated changes in  $\mu_a$  for (a) the upper compartment and (b) the corresponding lower compartment based on the experimental data shown in Fig. 4(a). The two compartments were separated at depth  $z_s$  (between 6 and 18 mm). In all cases  $\mu'_s = 1 \text{ mm}^{-1}$  and  $\mu_a = 0.02 \text{ mm}^{-1}$  were assumed.

for  $\mu_a$  values of 0.01, 0.02, and  $0.03 \text{ mm}^{-1}$ , i.e., a variation that sufficiently covers the range expected for NIR wavelengths. In all cases a thickness of the upper compartment of  $z_s = 12 \text{ mm}$  was assumed and a scattering coefficient of  $\mu'_s = 1 \text{ mm}^{-1}$ . Again, the  $\Delta\mu_a$  time course of the upper compartment is hardly affected by the choice of parameters. For the lower compartment, however, there is a strong variation in magnitude that can be explained by the strong decline in the  $m_j$  sensitivity for deeper layers when the absorption coefficient is increased (see Figure 2). Again, the recovery to the baseline directly after the bolus peak is influenced by the variations in background absorption. In a similar way, varia-

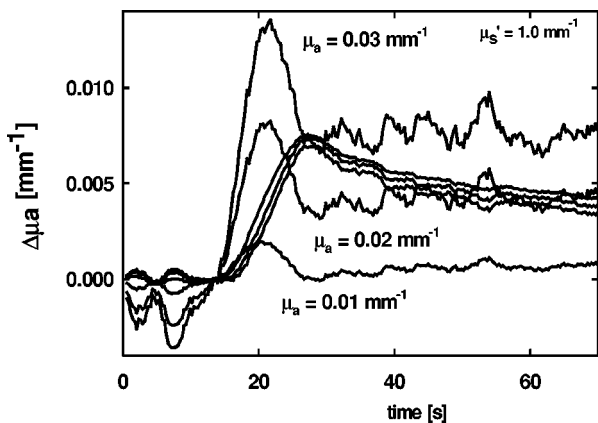


**Fig. 6** Calculated changes in  $\mu_a$  for an upper layer and the corresponding lower layer for the data of Fig. 4(a). For the calculation  $\mu_a = 0.01, 0.02, \text{ and } 0.03 \text{ mm}^{-1}$  were assumed. In all three cases the two layers were separated at a depth  $z_s = 12 \text{ mm}$ ;  $\mu'_s$  was  $1 \text{ mm}^{-1}$ .

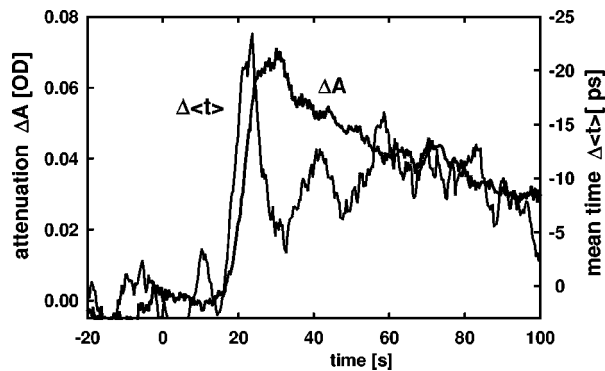


**Fig. 7** Raw data of  $\Delta\langle t \rangle$  and  $\Delta A$  averaged over two ICG boli injected at  $t=0 \text{ s}$  measured in an adult volunteer. The data are consistent with a faster and shorter bolus signal in the brain that is primarily detected by the mean time-of-flight signal compared to a slower bolus signal in the skin and skull primarily measured by intensity changes.

tions in the scattering coefficient of the model tissue were considered. By changing  $\mu'_s$  from 1 to  $2 \text{ mm}^{-1}$  the effect is by and large on the magnitude of the calculated  $\Delta\mu_a$  changes only (data not shown).

The shape of the bolus signal strongly varied among different volunteers. In some experiments there was no apparent difference between the time course of attenuation and the mean time of flight with a response similar to the attenuation data shown above. In other data sets the short bolus was already apparent in the raw data of the  $\Delta\langle t \rangle$  signal. An example is given in Figure 7, where  $\Delta\langle t \rangle$  has a clear ICG peak of about 10 s width that is earlier by more than 5 s compared to  $\Delta A$ .

To further describe the bolus signals the rising edge was analyzed as outlined in Figure 8(a). The raw data of  $\Delta A$  or  $\Delta\langle t \rangle$  were first approximated by a polynomial of fifth order between the time of injection and time of maximal ICG signal. From these smoothed lines, the rise time  $t_r$  defined as the difference between the 10% and 90% points in  $\Delta A$  or  $\Delta\langle t \rangle$  were obtained. Furthermore, based on the polynomial fit, the time of the maximal slope  $t_{ms}$  was calculated. For each subject  $t_{ms}$  and  $t_r$  were determined and gave mean values of  $\langle t_{ms}(\Delta A) \rangle = 20.5 \pm 5.5 \text{ s}$  and  $\langle t_r(\Delta A) \rangle = 10.7 \pm 3.5 \text{ s}$  for attenuation and  $\langle t_{ms}(\Delta\langle t \rangle) \rangle = 18.4 \pm 3.5 \text{ s}$  and  $\langle t_r(\Delta\langle t \rangle) \rangle = 10.4 \pm 4.1 \text{ s}$  for the mean time of flight. In Figure 8(b) the differences in  $t_{ms}$  and  $t_r$  for attenuation and mean time of flight data are shown for all subjects. While there is no significant difference in the mean rise time [ $\Delta\langle t_r(\Delta A, \Delta\langle t \rangle) \rangle = 0.3 \pm 2.5 \text{ s}$ ], evaluation of the time of maximal slope does indicate a more pronounced difference [ $\Delta\langle t_{ms}(\Delta A, \Delta\langle t \rangle) \rangle = 2.1 \pm 3.1 \text{ s}$ ] for the two measurement parameters.

The finding that analysis of  $\Delta A$  and  $\Delta\langle t \rangle$  allows different tissue compartments to be separated is further supported by data previously measured in babies during a cardiac pulmonary by-pass (CPB) operation.<sup>16</sup> In these babies ICG was injected into the CPB circuit at concentrations of 0.1 mg/kg body weight. It was found that the shape of the bolus time course of  $\Delta A$  and  $\Delta\langle t \rangle$  is very similar (see the example for a 13 week old baby in Figure 9) with no apparent differences in the ICG arrival time or bolus width. The likely explanation is that in babies the skin and skull are thin and therefore both

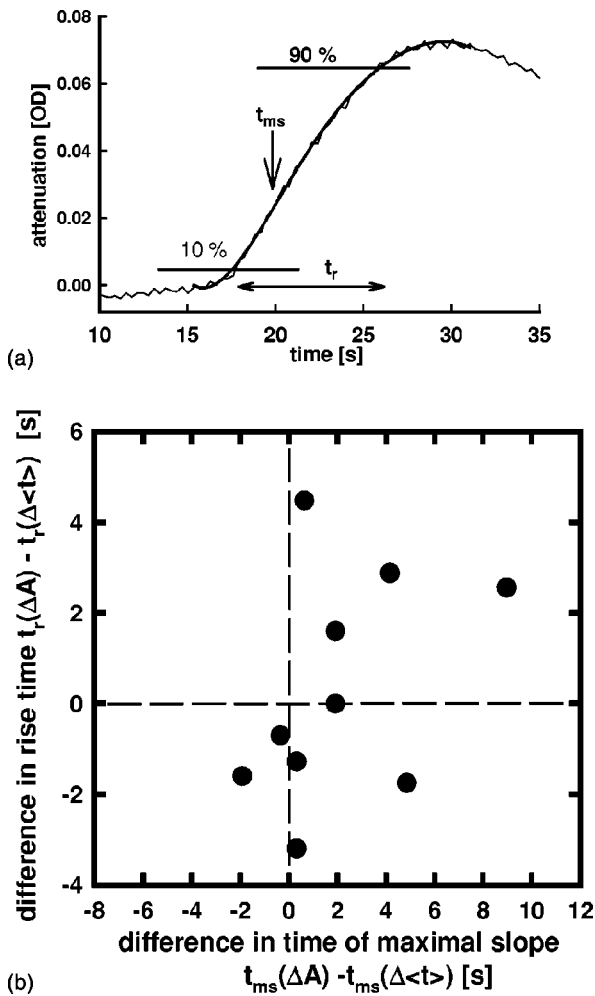


**Fig. 8** (a) Evaluation of rise time  $t_r$  defined as the difference between 10% and 90% points of the ICG induced attenuation increase and time of maximal slope  $t_{ms}$ . (b)  $t_{ms}(\Delta A) - t_{ms}(\Delta\langle t \rangle)$  vs  $t_r(\Delta A) - t_r(\Delta\langle t \rangle)$  for measurements in adult volunteers.

optical measurement parameters sample predominantly cerebral tissue with only small contributions from extracerebral compartments (cf. Figure 2).

The separation of extra- and intracranial bolus signals was also attempted by analyzing multidistance measurements ( $r = 10, 20, 30,$  and  $40$  mm). An example of bolus time courses is shown in Figure 10 for source–detector separations of 10 and 30 mm. The signals are similar with a slightly higher amplitude for the larger separation. The assumption is that at larger distances a larger signal is sampled from deeper layers and at the same time a moderately larger signal from layers close to the surface (cf. Figure 2). The concentration changes ( $\Delta c$ ) of both separations were first arbitrarily scaled to give similar overall signal magnitudes and then subtracted. When a scaling factor of 1.3 is used, the time course of  $\Delta c(30\text{ mm}) - \Delta c(10\text{ mm})$  1.3 peaks about 25 s after bolus injection with values close to zero for larger times. This is consistent with a greater depth sensitivity for the larger interoptode distance (IOD) (see Figure 2). However, the choice of scaling factor is somewhat arbitrary. It is consistent with the physical model (Figure 2) only when assuming  $z_s = 2\text{ mm}$  [ $I_j(z=0-2\text{ mm})$

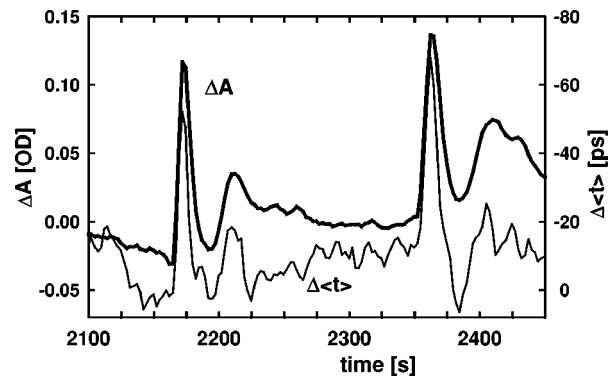


**Fig. 9** Changes in attenuation and mean time of flight following two ICG injections measured on the head of a 13 week old baby during cardiac by-pass operation (see Ref. 16).  $\lambda = 806\text{ nm}$ ,  $r = 30\text{ mm}$ . For both injections ( $t = 2166$  and  $2298\text{ s}$ ) the second passage of the dye is visible.

$= 17.94$  and  $14.65\text{ mm}$  for  $r = 30$  and  $10\text{ mm}$ , respectively]. Slight variations in  $z_s$ , i.e., in the thickness of the skin, result in large changes in the scaling factor derived from the Monte Carlo model. While for separations based on  $\Delta A$  and  $\Delta\langle t \rangle$  variations in  $z_s$  (Figure 5),  $\mu_a$  (Figure 6) or  $\mu'_s$  have a minor influence on the time course of the bolus signals, similar variations strongly affect the multidistance approach. Introducing a model derived rather than arbitrary scaling is therefore not justified as long as there are not precise data on the tissue’s optical properties and anatomy. In most of the data we found the analysis based on multidistance attenuation data to be unreliable for the recovery of peak bolus time courses when based on pathlength estimates as shown in Figure 2.

#### 4 Discussion

The data presented here demonstrate the capability of NIRS to noninvasively monitor cerebral perfusion in the human adult based on an ICG-bolus tracking technique similar to the Gd-DTPA bolus technique established for MRI. While in simple intensity measurements the signal from the cortex is masked by that from the skin and skull, the application of frequency-

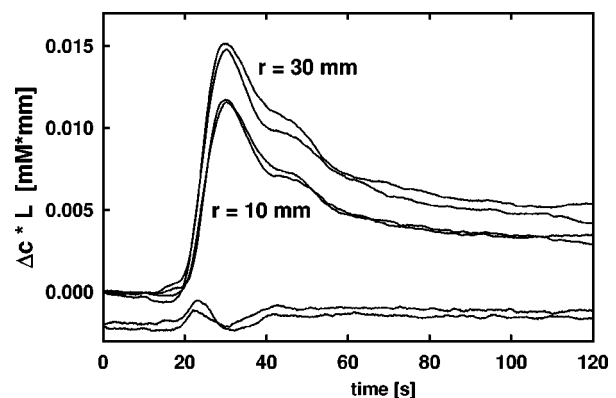


**Fig. 10** ICG concentration changes  $\Delta c$  at interoptode distances of  $r = 30$  and  $10\text{ mm}$  for two consecutive bolus injections (injection times set to  $t = 0\text{ s}$ ). In the lower section the traces  $\Delta c(30-10\text{ mm})$  1.3 are shown. For graphical reasons an offset of  $-0.002$  was chosen.

domain measurements in combination with a model based analysis allows the signals from an upper layer corresponding to the skin and skull and a lower layer that reaches the cerebral cortex to be separated. In volunteers it was regularly found that the arrival of the bolus signal is delayed in the upper layer (skin and skull) compared to in the lower layer. This is consistent with a lower perfusion rate and a longer retention time in the skin compared to the brain which is one of the most perfused organs. This finding is supported by analysis of MRI-perfusion data, which show a similar difference between the MTT in extra versus intracerebral tissue (Figure 1). Such a measure for extra- and intracerebral perfusion with a bedside method is of great potential relevance for the monitoring of vascularly diseased or traumatized patients. It should be noted that the approach presented here is not an alternative but may serve as an extremely helpful extension to the MTT assessment performed by Gd-DTPA enhanced functional MRI. Since the two techniques allow simultaneous application there is the perspective of an initial combined approach that is followed up on the intensive care or stroke unit at short intervals. The initial delay between the extra- and intracerebral bolus will serve as a baseline. To offset the effect of skin perfusion changes, a multisite measurement may be required. Changes of this delay may readily be explained by worsening or normalization of cerebral perfusion in the tissue illuminated. We are currently exploring the technique described here in patients undergoing cardiac by-pass surgery.

Our data suggest that more demanding time- or frequency-domain equipment is a prerequisite for reliable monitoring. However, preliminary measurements with a multisource multidetector topography system based on pure intensity data indicate that the spatial resolution might offset a lack of depth resolution (these data will be discussed in a separate paper). For reliable monitoring the combination of multisite and frequency- (time-) domain measurements seems even more desirable.

The core argument for the potential to differentiate between the extracerebral and the truly intracerebral compartments is the differences between the bolus shape and their relative latency. However, we regularly observed slow oscillations, best seen in the unaveraged data (see, e.g., Figures 6 and 7) with frequencies close to 0.1 Hz. They are much more prominent in the  $\Delta\langle t \rangle$  traces compared to in the  $\Delta A$  traces. The oscillations have recently been examined by NIRS<sup>17</sup> and are likely a cortical phenomenon, thus providing an additional argument for the stronger contribution of cerebral hemodynamics to the  $\Delta\langle t \rangle$  measurements. Another argument can be given by a comparison between the data from infants and adults. The lack of a delay between the two measurement parameters in infants corresponds to their much thinner skull and skin, and provides an anatomical explanation for this difference from adults.

### Acknowledgments

The data in Figure 9 are part of a study done at the Hospital for Children, Great Ormond Street (London, UK) by M. Kohl,

R. Watson, M. Cope, I. Roberts, G. Chow, and D. T. Delpy. This work was supported by the Deutsche Forschungsgemeinschaft (DFG).

### References

1. I. Roberts, P. Fallon, F. J. Kirkham, A. Lloyd-Thomas, C. Cooper, R. Maynard, M. Elliot, and A. D. Edwards, "Estimation of cerebral blood flow with near infrared spectroscopy and indocyanine green," *Lancet* **342**, 1425 (1993).
2. I. Roberts, P. Fallon, F. J. Kirkham, P. M. Krishbom, C. Cooper, M. Elliot, and A. D. Edwards, "Measurement of cerebral blood flow during cardiopulmonary bypass with near-infrared spectroscopy," *J. Thorac. Cardiovasc. Surg.* **115**, 94–102 (1998).
3. T. Kusaka, K. Isobe, K. Nagano, K. Okubo, S. Yasuda, M. Kondo, S. Itoh, and S. Onishi, "Estimation of regional cerebral blood flow distribution in infants by near-infrared topography using indocyanine green," *Neuroimage* **13**, 944–952 (2001).
4. W. M. Kuebler, A. Sckell, O. Habler, M. Kleen, G. E. H. Kuhnle, M. Welte, K. Messmer, and A. E. Goetz, "Noninvasive measurement of regional cerebral blood flow by near-infrared spectroscopy and indocyanine green," *J. Cereb. Blood Flow Metab.* **18**, 445–456 (1998).
5. G. J. K. Wietasch, F. Mielck, M. Scholz, T. von Spiegel, H. Stephan, and A. Hoelt, "Bedside assessment of cerebral blood flow by double-indicator dilution technique," *Anesthesiology* **92**, 367–375 (2000).
6. E. Keller, G. Wietasch, P. Ringleb, M. Scholz, S. Schwarz, R. Stinglele, S. Schwab, D. Hanley, and W. Hacke, "Bedside monitoring of cerebral blood flow in patients with acute hemispheric stroke," *Crit. Care Med.* **28**, 511–516 (2000).
7. P. W. McCormick, M. Stewart, and M. Goetting, "Noninvasive cerebral optical spectroscopy for monitoring cerebral oxygen delivery and hemodynamics," *Crit. Care Med.* **19**, 89–97 (1991).
8. P. W. McCormick, M. Stewart, G. Lewis, M. Dujovny, and J. I. Ausman, "Intracerebral penetration of infrared light," *J. Neurosurg.* **76**, 315–318 (1992).
9. E. Okada, M. Firbank, M. Schweiger, S. R. Arridge, M. Cope, and D. T. Delpy, "Theoretical and experimental investigation of near-infrared light propagation in a model of the adult head," *Appl. Opt.* **36**, 21–31 (1997).
10. S. R. Arridge, "Photon-measurement density functions. Part I: Analytical forms," *Appl. Opt.* **34**, 7395 (1995).
11. J. Steinbrink, "Nahinfrarotspektroskopie am Kopf des Erwachsenen mit Pikosekunden-Zeitaufloesung," PhD thesis, Berlin, 2000.
12. J. Steinbrink, H. Wabnitz, H. Obrig, A. Villringer, and H. Rinneberg, "Determining changes in NIR absorption using a layered model of the human head," *Phys. Med. Biol.* **46**, 879–896 (2001).
13. S. J. Matcher, M. Cope, and D. T. Delpy, "In vivo measurements of the wavelength dependence of tissue-scattering coefficients between 760–900 nm measured with time-resolved spectroscopy," *Appl. Opt.* **36**, 386–396 (1997).
14. S. R. Arridge, M. Cope, and D. T. Delpy, "The theoretical basis for the determination of optical pathlengths in tissue: Temporal and frequency analysis," *Phys. Med. Biol.* **37**, 1531–1560 (1992).
15. K. Uludag, M. Kohl, J. Steinbrink, H. Obrig, and A. Villringer, "Crosstalk in the Lambert–Beer calculation for near-infrared wavelengths estimated by Monte Carlo simulations," *J. Biomed. Opt.* **7**, 51–59 (2002).
16. M. Kohl, R. Watson, G. Chow, I. Roberts, D. T. Delpy, and M. Cope, "Monitoring of cerebral hemodynamics during open-heart surgery in children using NIR phase resolved spectroscopy," *Proc. SPIE* **2979**, 408–416 (1997).
17. H. Obrig, M. Neufang, R. Wenzel, M. Kohl, J. Steinbrink, and A. Villringer, "Spontaneous low frequency oscillations of cerebral haemodynamics and metabolism under rest and visual stimulation in adults," *Neuroimage* **12**, 623–639 (2000).